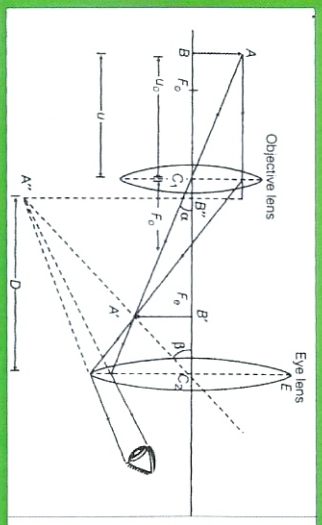

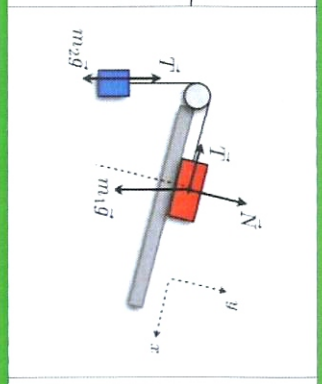

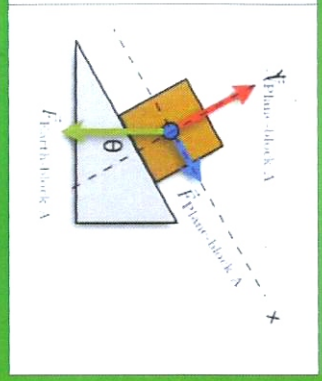

KADA
Journal of Physics

Vol. 1 (1) April, 2017 ISSN: 2579-1168

A Publication of
Department of Physics,
Faculty of Science,
Kaduna State University

DEPARTMENT OF PHYSICS,
FACULTY OF SCIENCE,
KADUNA STATE UNIVERSITY, KADUNA - NIGERIA

TABLE OF CONTENTS

Synthesis, Structure and Electrical properties of NASICON ($LiSn_{2-x}Ti_x(PO_4)$ (x=0.4) Ceramic

Umaru Ahmadu[1], KasimUthman Isah[1], Abdullahi Mann[2]Ibrahim, S.O.[1]and Mohammed Isa Kimpa[1,3]
[1]Department of Physics, Federal University of Technology, Minna, Nigeria
[2]Department of Chemistry, Federal University of Technology, Minna, Nigeria
[3]Department of Science, Faculty of Science, Development and Human Resources, University Tun Hussein Onn Malaysia, BatuPahat, Jo

ABSTRACT

$LiSn_{1.6}Ti_{0.4}(PO_4)$ ceramic powder was synthesized via solid state reaction and investigated for electrical and dielectric properties for use as solid electrolyte. X-ray diffraction shows that it has rhombohedral $R\bar{3}c$ NASICON-type structure with unreacted phase of SnO_2. Impedance study in the temperature range 300 to 740 K and frequency range 300 kHz-3 GHz were carried out together with dielectric permittivity studies under the same conditions. The determined bulk and grain boundary conductivities are 1.39 x 10^{-3} S/cm and 3.39 x 10^{-4} S/cm at 740 K, respectively, while their corresponding room temperature conductivities are 6.31 x 10^{-6} S/cm and 1.72 x 10^{-6} S/cm, respectively. Activation energies determined from Arrhenius plot are 0.67 eV and 0.78 eV for bulk and grain boundary, respectively. The determined dielectric constant ε' has a value of 40 at 303 K and reached a maximum of 1790 at 740 K, which is high compared to most reported values for NASICON and indicate that $LiSn_{1.6}Ti_{0.4}(PO_4)$ could be a promising candidate for application as solid electrolyte at elevated temperatures.

Keywords: *NASICON; conductivity; permittivity; impedance; solid electrolyte*

INTRODUCTION

Conventional battery systems contain liquid electrolytes, have high ionic conductivities and offer very good contact with electrodes but have major setbacks such as cell leakage, self-discharge, drying out of the cell, loss of electrolyte, corrosion and environmental concerns,all of which grossly limit their long–term life cycles. Solid electrolytes on the other hand can overcome most of these challenges. Lithium ion rechargeable batteries are solid electrolytes that are considered good materials for large scale energy storage due their high energy density and flexibility. However, current lithium ion battery technology still has several weaknesses such as low conductivity and mechanical strength, limitations of working voltage and overheating (or combustion), all of which have heightened the importance of safety in battery technology. Batteries based on lithium show the best performance and thus a lot of research has been carried out on the synthesis and characterisation of Li based materials due to their low weight, small ionic radii, high open circuit voltage and potential use in high energy density batteries (Lakshmi & Govindaraj 2009). Many researches have been tailored toward enhancing the thermal, electrochemical, mechanical and electrode–electrolyte contact resistance properties, among others.The investigation of NASICON (Sodium superionic conductor) materials for solid electrolyte application is one key research area. This family of compounds has a unique structure resulting from its composition which confers on it varied physical-chemical properties (Ahmadu 2014; Venkateswara *et al.* 2014) such as high sodium conductivity, low thermal expansion coefficient, chemical stability and catalytic activity, amongst others. Ionic conductivity of NASICON is of the order of 10^{-3} S/cm, which is high, compared to those of liquid electrolytes (Ahmadu *et al.* 2009). Depending on the composition, the crystal structure can exist in different polymorphs *i.e.*,

rhombohedral, orthorhombic, monoclinic and triclinic with different space groups $R\bar{3}c$, $P21/n$ and Cc.$LiSn_2(PO_4)_3$ is a member of the NASICON family and a *Li^+ ion conductor studied for its efficiency as anode material (Martinez et al 1994)for lithium ion rechargeable batteries but the least studied. It has two crystallographic phases, a high temperature rhombohedral $R\bar{3}c$ structure with high ionic conductivity and a low temperature triclinic P1or monoclinic Cc structure with low conductivity(*Martinez*et al.* 1997*) and high melting point above 1923K (Kumar &Yashonah 2006)* .One of the challenges in NASICON-type material for solid electrolyte application is achieving a high conductivity at room temperatures. Impedance analysis shows that $LiSn_2(PO_4)_3$ sintered at 873 K has conductivity of 1.38×10^{-5} Scm^{-1}while that sintered at 923 K has lower conductivity of 1.03×10^{-5} Scm^{-1}. The sample sintered at 873 K shows the highest bulk conductivity of 10^{-6} Scm^{-1} at 303 K and 10^{-5} Scm^{-1} at 773 K in comparison to that sintered at 923 K. The ionic conductivity obtained is higher, compared to that reported by Norhaniza *et al.*(2010).The Arrhenius plot shows bulk activation energy of 0.005 eV for sample with highest conductivity in the low temperature region, and 0.250 eV in the high temperature region. The low activation energy was attributed to uniform diffusion channels in the NASICON structure (Narváez-Semanate& Rodrigues 2010).*However, the stability of the pellets was a problem, though Norhaniza et al.(2010) have reported success in obtaining stable pellets of $LiSn_2(PO_4)_3$using mechanical ball milling with a higher ionic conductivity of $\approx 10^{-7}$ S cm^{-1}at room temperature.*

The bulk (σ_b) conductivity is deduced from eqn. (1).

$$\sigma_b = \frac{d}{AR_b} \qquad (1)$$

where d is the sample thickness and A the cross sectional area of the sample and R_b the bulk resistance. Measurement of bulk conductivity is usually straight forward from the Nyquist plots while the measurement of specific grain boundary conductivity requires knowledge of the grain size and grain boundary thickness. In order to determine the grain boundary conductivity without detailed microstructural and electrical information the 'Brick Layer Model' (BLM) is used(Bonanos *et al*2005; Ahmadu *et al* 2010). In the current case, it was deduced from the impedance and conductivity plots by extrapolation to the real Z' or σ' axes, as the case may be. Traditionally, impedance has been measured in the radio frequency range, however, the GHz technique offers an entirely new approach apart from its high temperature use (Kezionis *et al* 2011).The electrical model of impedance used is that of an ideal polycrystalline sample where the Nyquist plot exhibits an arc at high frequency, a second arc at low frequency and a linear portion at the lowest frequency. Two parallel RC circuits represent the two semicircles which are in series with a constant phase element representing the lowest frequency (the electrode characteristics). The Arrhenius expression is commonly used to deduce activation energy at any temperature (T)and is given by eqn. (2).

$$\sigma = (A/T)\ exp\ (-E_a/kT) \qquad (2)$$

where k is the Boltzmann's constant, E_a is the electrostatic energy (i.e. activation energy) barrier which the ion has to overcome in order to jump from one site to another in the crystal and A is called pre-exponential factor and contains all the remaining factors that influence ionic conductivity. The frequency dependence of conductivity can be evaluated from the dielectric data from the relation $\sigma_{ac} = \omega\varepsilon_0\varepsilon'' tan\delta$ where σ_{ac} is the ac conductivity, ω is the angular frequency $(2\pi f)$,$\varepsilon_0$is the permittivity of free space ($8.854 \times 10^{-14}$$Fcm^{-1}$), $\varepsilon''$is dielectric loss(imaginary part of dielectric permittivity) and $tan\delta$ is the loss tangent factor. The ac conductivity of materials at a given temperature obeys the universal power law, $\sigma_{ac}=\sigma_{dc}+A\omega^n$ where σ_{ac} , σ_{dc} are ac and dc

conductivity of the material, respectively, A is a temperature dependent parameter, $\omega = 2\pi f$ and n is the power law exponent which represents the degree of interaction between the mobile ions and is less than 1. The value of n is extracted from the slope of log σ_{ac} versus log ω. The real and imaginary components of dielectric permittivity can be calculated from eqn.(3).

$$\varepsilon^* = \varepsilon' - \varepsilon'' \frac{1}{i\omega CZ^*} \quad (3)$$

In the present work, results of the preparation of Ti-doped $LiSn_2(PO_4)_3$ using solid state reaction have been presented. The chosen sintering parameters are expected to lead to an elucidation of their structural, thermal (based on TGA/DTA and X-ray diffraction) and electrical conductivity and dielectric properties using GHz impedance technique. It is also expected to lead to stability of the ceramics, thereby resolving some of the above problems.

MATERIALS AND METHODS

The materials used for the synthesis of Ti-doped $LiSn_2(PO_4)_3$are analytical grade lithium carbonate (Li_2CO_3, India,>99%), titanium oxide (TiO_2, BDH, 99.99%), stannous oxide(SnO_2, BDH, 99.99%), ammonium dihydrogen phosphate ($NH_4H_2PO_4$, BDH, 99.99%),methanol(CH_3OH, BDH, 99.99%) and Polyvinyl alcohol (PVA).Stoichiometric amounts of the mixtures were measured and preparation was carried out using solid-state reaction. Stoichiometric compositions were weighed, thoroughly mixed and ground using agate mortar and pestle for 8hrs.Ethanol (C_2H_2OH) was added to the mixture to aid homogeneity.

Thermogravimetric analysis measurements were carried out using model TGA 4000 Perkin Elmer (USA). 0.5g of sample was weighed into a small aluminium crucible. The pan was heated from 303to 1113K at a heating rate of 283K/min in air atmosphere. The weight loss was determined from the TGA curves by means of Universal Analysis 2000 software. The sample was poured into an aluminium crucible, placed inside a furnace and calcined at 1173K for 4hrswhile the decomposition of volatile materials were observed (water, CO_2, and NH_4). The calcined sample was ground for 2hrsand pelletized.2 g of PVA was mixed in 2ml distilled water for use as binder. To get a clear solution the distilled water was boiled on a hot plate. The mixture was put into a mould of diameter of 16 mm by 1.7mm thickness and pressed for 5 mins in a hydraulic press of 5 N/m^2pressure to form pellets. The pellets were put into a furnace and sintered at 1173K for 3hrs and allowed to furnace-cool to room temperature. Thereafter, it was re-ground for 2hrs and pelletized. The pellets were then sintered at temperature of 1273K for 3hrs and allowed to cool to room temperature. This procedure was repeated at 1373K, followed by regrinding and pelletizing for characterisation.

Thermal behaviour of the sample was analysed at a constant heating rate of 10 $Kmin^{-1}$ in the temperature range 303to 1113K in air atmosphere. Both DTA/TGA data were automatically acquired from the machine. Structure and phase analyses of the sample were performed by X-ray Diffractometer (D8 Advance, BRUKER AXS, 40 kV, 40 mA) with monochromatic CuK1(λ = 1.54060 Å) radiation using a step scan mode of step size 0.034 ° and counts were accumulated for 88 s at each step for 2θ values ranging from 20 ° to 90 °.The crystallite size (D) was calculated using the Scherer eqn. (4).

$$D = \frac{k\lambda}{\beta \cos\theta} \quad (4)$$

where k is the Scherer constant (0.94),λ is the wavelength of the X-ray source, β is Full Width at Half Maxima (FWHM) in radians, θ is Bragg's angle (in radians).

The sintered ceramics were mounted on an aluminium stage with the aid of carbon adhesive tape and coated with AuPd (Gold-Palladium) using a sputter coater. High Resolution Scanning Electron Microscope

(HRSEM, Zeiss) coupled with an Energy Dispersive Spectrometer (EDS) was employed to record and analyse the surface morphology and elemental compositions of the samples. The instrument was operated at a voltage of 20 kV and images were captured at 5 kV. Due to poor density and stability the samples were further heated to 1573K and then annealed to room temperature to improve their mechanical properties. Impedance measurements were carried out by measurement of complex impedance ($Z = Z' - iZ''$) and complex electric conductivity ($\sigma = \sigma' - i\sigma''$) of the samples using coaxial impedance spectrometer (Kežions *et al.*, 2011) set-up in the frequency range 300 kHzto3GHz.Measurements were taken every 10 K on heating the sample at 1 K per min using a fixed voltage of 200 mV in air atmosphere. The samples were covered with platinum electrode paste and heated to 1073 K. The control and acquisition of data were carried out using Origin graphing software. Temperature range of 300 to 740K was used for all measurements. The dielectric constant (ε') and dielectric loss (ε'') of the sample were calculated using eqns. (5) and (6).

$$\varepsilon' = Z'/wC_o(Z'^2 + Z''^2) \quad (5)$$

$$\varepsilon' = Z'/wC_o(Z'^2 + Z''^2) \quad (6)$$

where, Z' and Z'' are the real and imaginary impedance, $w = 2\pi f$ and $C_o = \varepsilon_o \frac{A}{d} \varepsilon_o =$ permittivity of free space, $8.854 \times (10^{-14} Fcm^{-1})$, A= area of sample and d = sample thickness

RESULTS

The results of the TGA/DTA runs for $LiSn_{1.6}Ti_{0.4}(PO_4)_3$ are shown (Fig.1) as curves in a dual axes plot. The red curve is the TGA while the blue cure represents the DTA. The curves have been used to study the thermal properties of NASICON ceramics (Ahmadu *et al.* 2010).

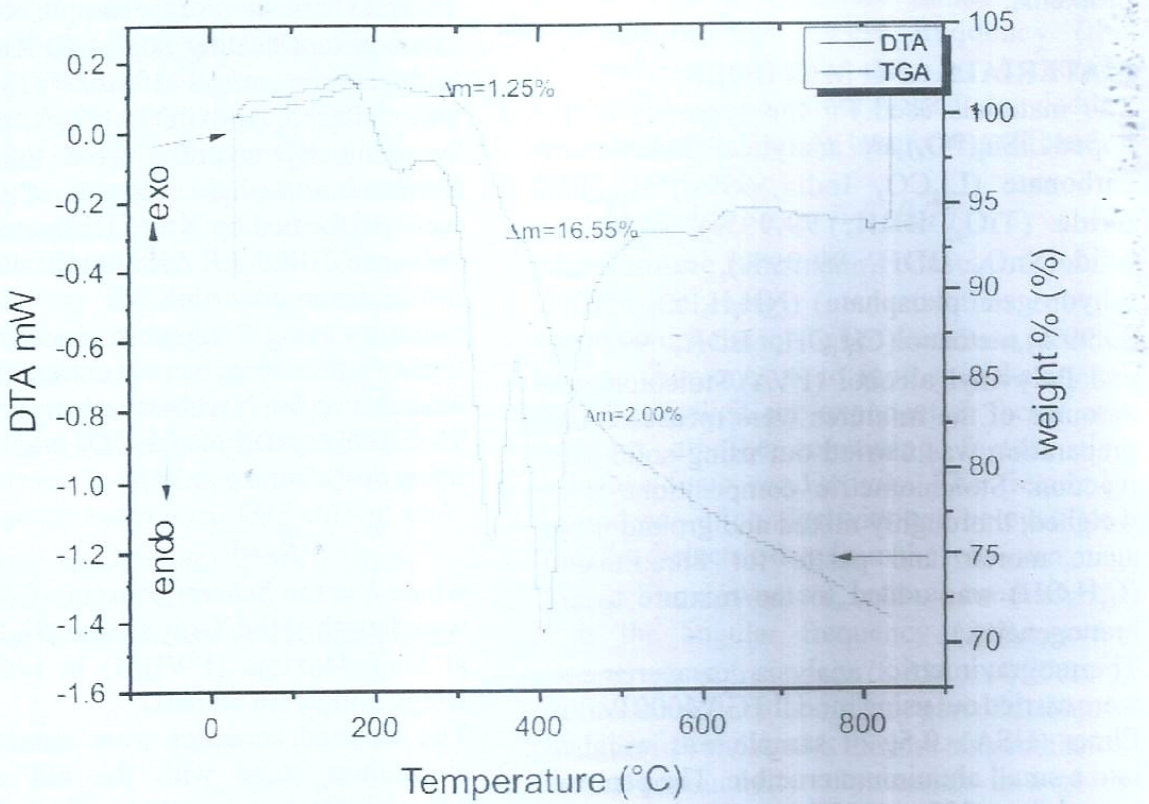

Figure 1 TGA/DTA curve of $LiSn_{1.6}Ti_{0.4}(PO_4)_3$ showing decomposition and transitions.

The results of X-ray diffraction show pattern of polycrystalline $LiSn_{1.6}Ti_{0.4}(PO_4)_3$ in Fig. 2.

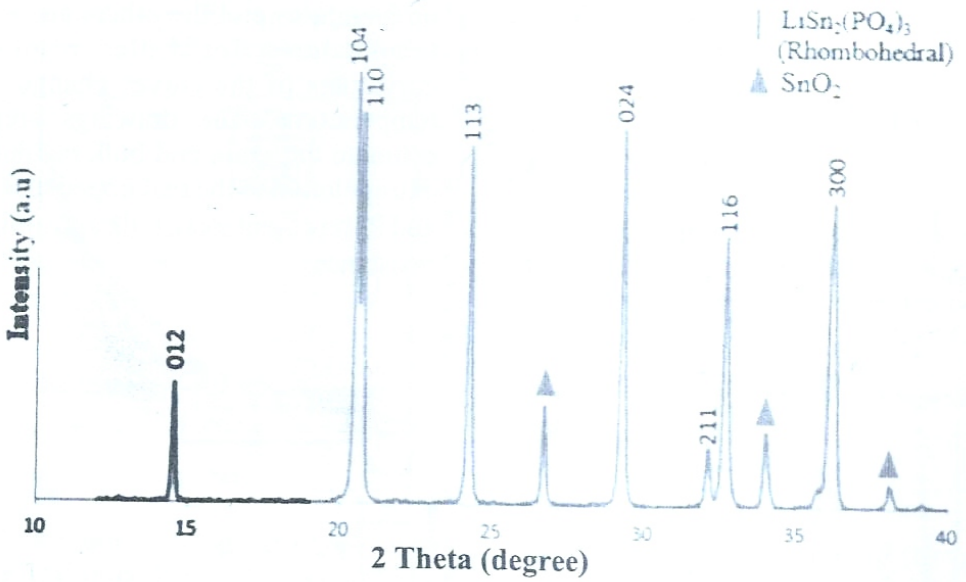

Fig. 2. XRD pattern of sintered $LiSn_{1.6}Ti_{0.4}(PO_4)_3$ with peaks of unreacted SnO_2 in the 2Θ range indicated.

The red icon represents unreacted SnO_2 detected. Calculated lattice parameters, unit cell volume and crystallite size of the sample are presented in table 1 and indicate the formation of solid solution. Table 2 is a comparison of experimental and theoretical densities of the samples and shows that the densities are more than 86 % of their theoretical values (3.42 gcm^{-3}).

Table 1. Lattice parameter, cell volume and average crystallite size of samples

Sample(x)	a(A°)	b(A°)	c(A°)	V(A°^{3})	Average Crystallite size (nm)
$LiSn_{1.60}Ti_{0.40}(PO_4)_3$	8.6466	8.6466	21.0426	1362.45	1.99

Table 2 . Comparison of experimental and theoretical densities of the samples

Sample(x)	Experimental(g/cm^3)	Theoretical(g/cm^3)	(%)
$LiSn_{1.60}Ti_{0.40}(PO_4)_3$	2.94	3.42	86.07

Fig 3 is the qualitative EDX spectrum of the detected elements. The quantitative results are presented in table 3 and indicate the presence of Sn, P, O, Ti and C in the sample.

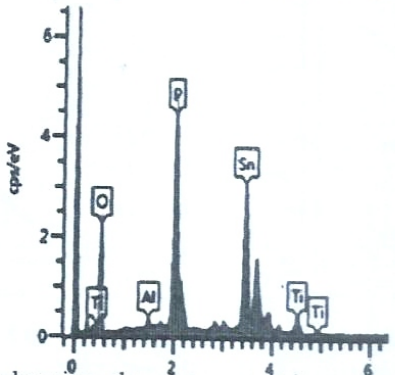

Fig. 3. EDX spectra showing element present in powered $LiSn_{1.60}Ti_{0.40}(PO_4)_3$

Table 3. Nominal and EDX–derived atomic concentrations of $LiSn_{1.60}Ti_{0.40}(PO_4)_3$

Sample	Stoichiometric atomic ratios			
	Sn	P	Ti	O
$LiSn_{1.60}Ti_{0.40}(PO_4)_3$	1.63	3.00	0.40	12.00
EDX	1.90	2.64	0.39	11.87

Fig.4(a-f) are the complex impedance spectra of the sample at different temperatures, where (a)is the composite plot at all the measured temperatures and the others are at individual temperatures for better resolution. The curvatures of the curves change at different temperatures. The drawings are meant to estimate the grain and bulk conductivities by extrapolation to the real impedance axis. R_t, R_b and R_g represent total, bulk and grain boundary resistance.

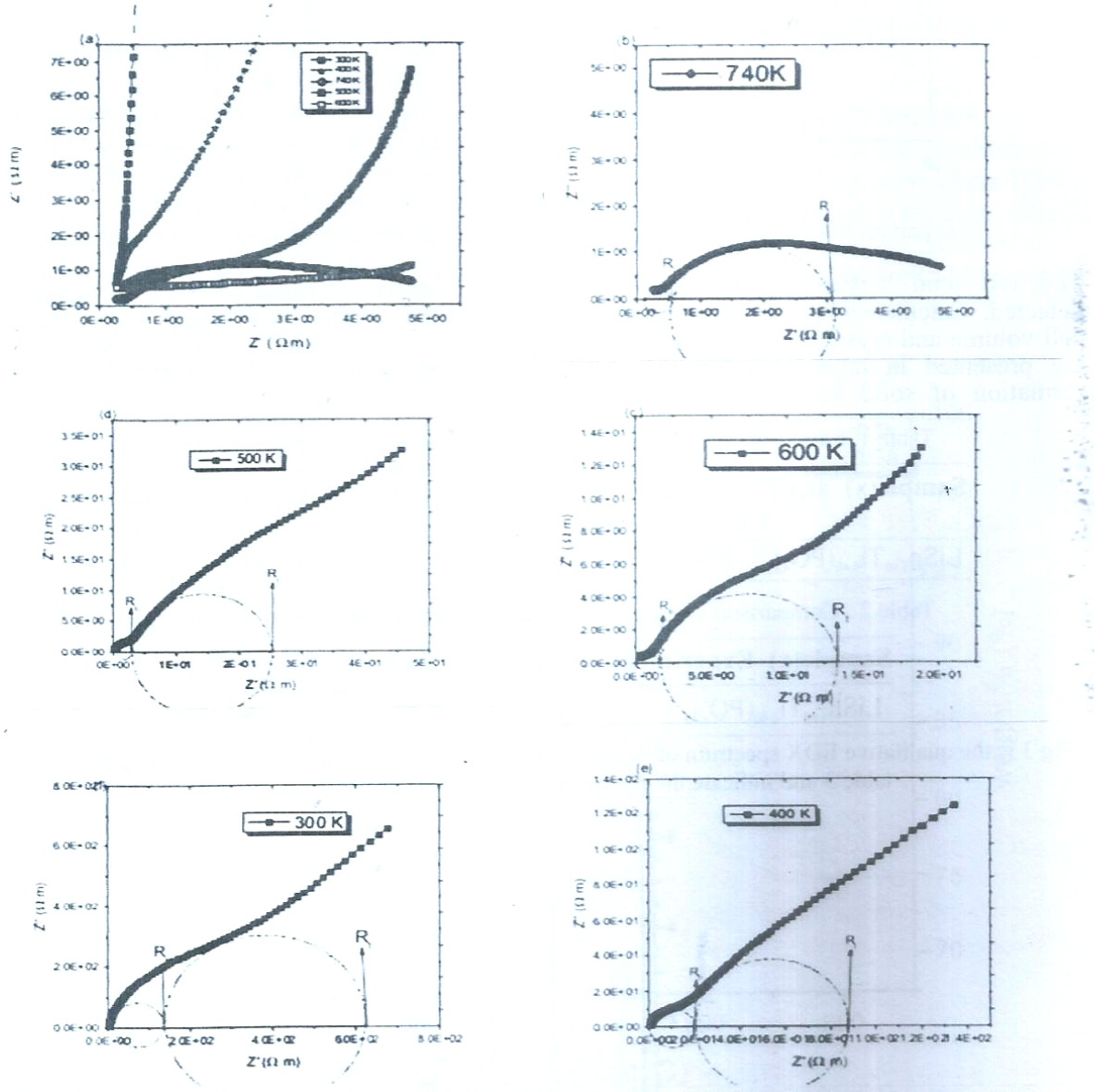

Fig. 4.(a) composite impedance plots of $LiSn_{1.6}Ti_{0.4}(PO_4)_3$ (300 to 740 K), (b)individual impedance plots for $LiSn_{1.6}Ti_{0.4}(PO_4)_3$ at temperatures 740 (c) 600 (d) 500 (e) 400 and (f) 300 K, showing the extrapolations for grain and grain boundaries.

Fig.5(a,b) represent the variations of the real and imaginary parts of impedance vs Log frequency at different temperatures (300 to 740 K)

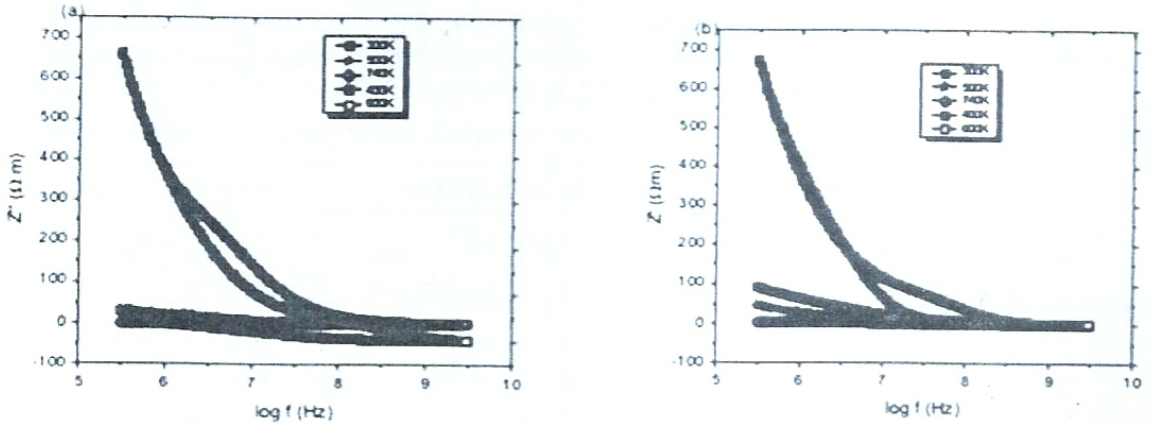

Fig. 5. (a) variation of imaginary impedance ($Z^{'}$) versus log of frequency (f) and (b) variation of real impedance ($Z^{''}$) versus log of frequency (f) at different temperatures.

Fig. 5(a-d) represents the complex conductivity plots (a-composite) at different temperatures. The circles and tangents enable one to deduce the total and bulk conductivities by extrapolation of the tangents to the real conductivity axis.

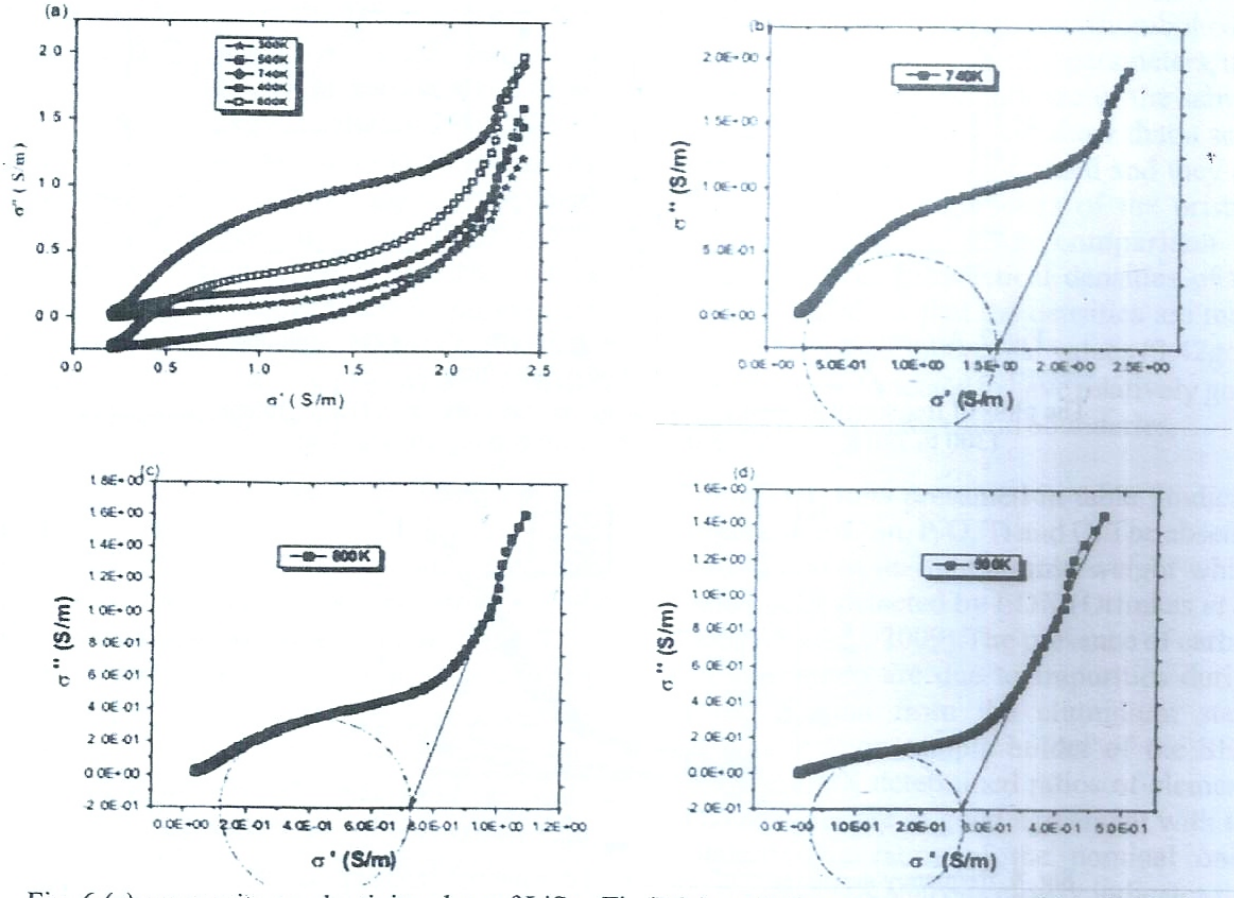

Fig. 6.(a) composite conductivity plots of $LiSn_{1.6}Ti_{0.4}(PO_4)_3$ at different temperatures (b) individual plot at 740 K © 600 K (d) 500 K.

Table 4 is a comparison of the conductivity deduced from impedance curves (dc conductivity) and that from complex conductivity (ac conductivity) and show close agreement.

The result obtained by comparing the values of bulk conductivity from impedance measurements, i.e., dc component, extrapolation of tangents, and that deduced from ac conductivity measurements (complex conductivity) is presented in table 4.

Table 4 .Comparison of the bulk (σ_b) conductivities from Z and σ plots at different temperatures

Temperature (K)	'plots σ_b (S/cm)	'plots (S/cm)
300	6.31×10^{-6}	5.00×10^{-5}
400	5.95×10^{-5}	4.30×10^{-4}
500	3.38×10^{-4}	2.65×10^{-3}
600	3.675×10^{-4}	7.40×10^{-3}
740	1.39×10^{-3}	1.55×10^{-2}

The plot of log σ versus 1000/T (Arrhenius plot) for both bulk and grain boundary in the temperature range from 300 to 740 K are shown in Fig. 8(a-b) where the red line is the fit, the black is the data point. It is a linear fit.

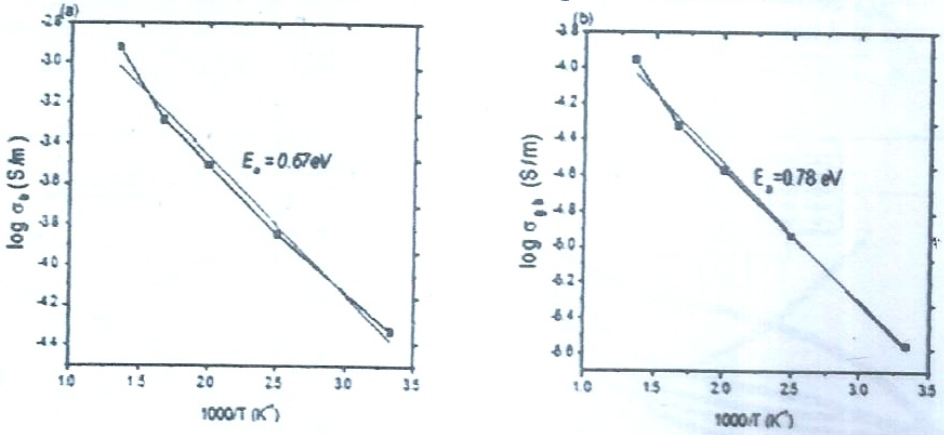

Fig. 7. Arrhenius plot of conductivity of $LiSn_{1.6}Ti_{0.4}(PO_4)_3$ (a) bulk conductivity and (b) grain boundary conductivity.

The plots of frequency dependence of the ac conductivity (σ vs f) at different temperatures (300 to 740 K) are shown in Fig.8 where two regions are clearly observed.

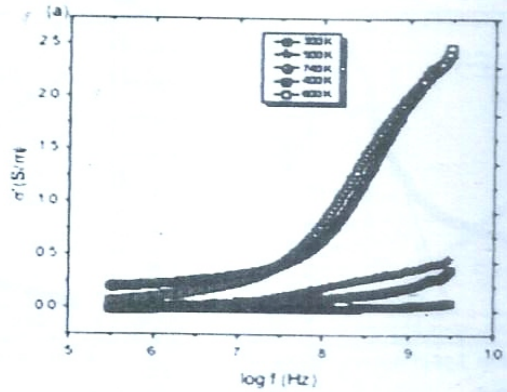

Fig. 8. frequency dependence of real part of conductivity and of $LiSn_{1.6}Ti_{0.4}(PO_4)_3$

The plot of frequency dependence of dielectric constant (ε'vs frequency) in the frequency range 300 kH to 3 GHz and dielectric loss (ε') in the same range are shown in Fig. 9(a-b) at different temperatures.

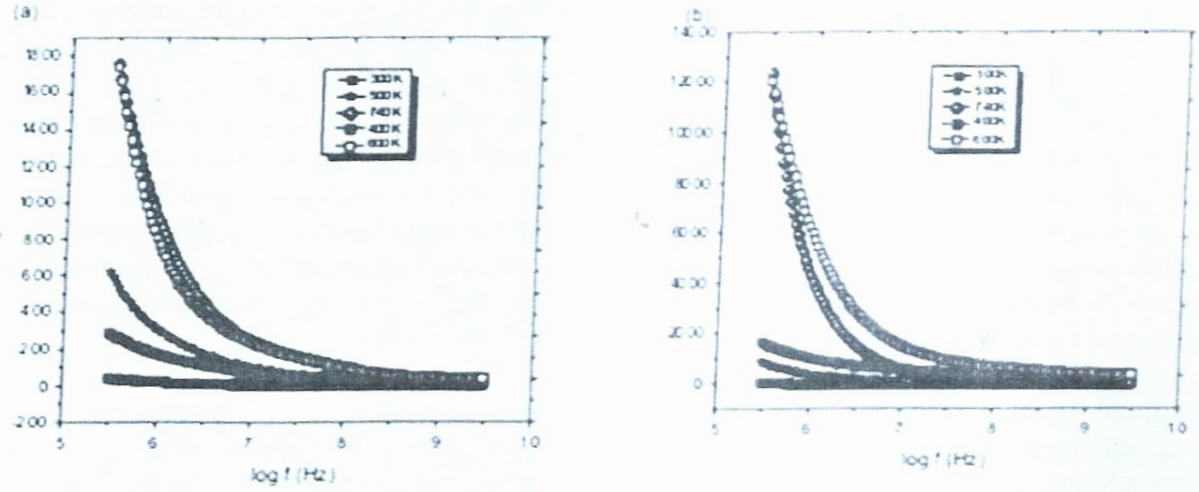

Fig. 9(a) frequency of real part of dielectric permittivity of $LiSn_{1.6}Ti_{0.4}(PO_4)_3$ and (b) frequency dependent part of imaginary part of dielectric permittivity

DISCUSSION

The plots in Fig.1represent the TGA/ DTA curves of $LiSn_{1.6}Ti_{0.4}(PO_4)_3$.Three main weight losses are observed in the TGA curve between 30to 250°C totalling ~1.25 %due to evaporation of water. The second weight loss of~17.05% is observed between 250 to 400°C and indicates the decomposition of ammonium (Krok 1987; Zhou & Ahmad 2007). The third weight loss rom400to 480°C has overall weight loss of~20.30% and is attributed to chemical reaction during the formation of $LiSn_{1.6}Ti_{0.4}(PO_4)_3$.The sintering temperature is therefore around 900°C(Ignazak *et al.* 2006).

The X-ray diffraction pattern of polycrystalline$LiSn_{1.6}Ti_{0.4}(PO_4)_3$ inFig.2clearly indicates the formation of rhombohedral NASICON-type structure of symmetry (R3c) for sintered $LiSn_{1.6}Ti_{0.4}(PO_4)_3$ with unreacted SnO_2 phase in agreement with the XRD pattern of $LiSn_2(PO_4)_3$ reported by other researchers (Martinez *et al.* 1994; Martinez *et al.* 1995; Norhaniza *et al.* 2011; Cui*et al.* 2012; Mustaffa *et al.* 2015) and with the ICSD 202157 card (1997). Aono *et al.* (1994) reported the presence of minor SnO_2 phase which they attributed to Li loss at high temperatures. Similarly, the lattice parameters*are similar* to those reported by other workers (Norhaniza *et al.* 2010; Norhaniza *et al.* 2011; Mustaffa *et al.* 2014; Mustaffa *et al.* 2015) for rhombohedral structure. The results of lattice parameters, unit cell volume and crystallite size of the sample are presented in table 1 and show that a solid solution has indeed been formed and they are within the lattice parameters of the pristine material. Table 2 is a comparison of experimental and theoretical densities of the samples and show that the densities are more than 86 % of their theoretical values (3.42gcm^{-3}) and hence is expected to have relatively good conductivity with less grain boundaries.

The EDX results presented in table 3indicate the presence of Sn, P, O, Ti and C. The absence of Li is due to its light atomic weight which could not be detected by EDX (Orlinkas *et al.* 2006; Wu *et al.*, 2009).The presence of carbon and aluminium are due to impurities during characterisation from the aluminium stage used and carbon sample holder of the SEM machine. EDX determined ratios of elements in all samples are in good agreement with the stoichiometric ratios of the nominal ones. Therefore, EDX analysis clearly indicates that titanium has been successfully substituted in

the $LiSn_2(PO_4)_3$ structure (Fig.3).

The complex impedance (Z) plots of $LiSn_{1.60}Ti_{0.40}(PO_4)_3$ at different temperatures(300 to 740K) shown in Fig.4(a-f) indicate that at low temperatures the material shows insulating properties (the curves are almost straight lines)and become curved at higher temperatures. As the temperature increases the curves become almost perfect semicircles and indicate an increase in conductivity of the sample. The plots have been separated as shown in Fig.4(b-f) for easy extrapolation of resistance values from the impedance plots. For each temperature, the values of bulk and grain boundary resistance (R_b, R_{gb}, respectively) were determined from the intercept of the high and middle frequency semicircle with the Z -axis which is obtained by extrapolating the curvy part of the arc to the Z axis of impedance plots. At 740K two deformed and partially overlapping semicircles are observed which are associated with the resistance of grains and grain boundaries (Ŝalkus *et al.* 2013).At 600 to 300 Ka small semicircle is observed at high frequency and an arc at the middle frequency (Mariappan & Govindaraj 2005).

Except for plot at 300 K, all the curves show an indication of grain and grain boundary components and the impedances gradually decrease with increase in temperature. The estimated values of the grain and grain boundary resistances are as shown in the plots. The values of bulk and grain boundary resistances and conductivities deduced by extrapolation from the curvy plots show that conductivity increases with increase in temperature. The highest conductivity determined are 1.39×10^{-3} S/cm and 3.39×10^{-4} S/cm for bulk and grain boundary at 740 K, respectively, while room temperature conductivities are 6.31×10^{-6} S/cm and 1.72×10^{-6} S/cm for bulk and grain boundary, respectively.
Fig.5(a-b) shows the frequency dependence of imaginary (Z) and real impedance (Z) in the range 300 to 740 K. The characteristics of all the plots are similar. In both cases the impedances decrease with increase in temperature and at high frequencies they become frequency independent. There is no relaxation observed in the temperature and frequency range investigated. The impedances are high at low frequencies and at temperatures 600 and 740 K.

Due to indistinguishable semicircles for bulk and grain boundary resistance in the impedance and ac conductivity spectrum they were deduced by extrapolating to the real part of the ac conductivity composite plot in Fig.6(a), by drawing tangents to the linear portions of the plots to intersect the semi-circular arcs at σ at axis of the individual plots at different temperatures. This gives the total conductivity. The bulk conductivity (σ_b) is obtained from the intercept of the dispersion curves with the real axis at high frequencies and total conductivity σ_t is obtained from the intercept with the curve at middle frequencies (Norhaniza *et al.* 2011; Adnan & Mohamed 2012) and is given by the relation, $\sigma_{gb} = \sigma_t - \sigma_b$ where, σ_t is total conductivity, σ_{gb} is grain boundary conductivity and σ_b is bulk conductivity.
Table 4indicates that the bulk (σ_b) conductivities from impedance and ac σ plots at different temperatures are in close agreement and are different due to the poor curvatures of the semi circles and the error in drawing the tangents to the arcs.

The variation of the dc conductivity with temperature has been plotted from the Arrhenius equation in the form of a linear plot of log σ versus 1000/T for both bulk and grain boundary, in the temperature range 300 to 740Kas shown in Fig.7(a-b).It is observed that both the bulk and grain boundary conductivities obey the Arrhenius law with regression values of 0.98 and 0.99 for σ_b and σ_{gb}, respectively. Their corresponding

activation energies are 0.67eV and 0.78eV, respectively. These values are higher compared to those reported in literatures (Winand *et al.* 1991; Martinez *et al.*1997), which are given as 0.34 and 0.55eV, respectively. The high activation energies are due to the sintering conditions and conductivity mechanisms which are important factors that affect σ_b, σ_{gb} and their respective activation energies (Chen *et al.*2009; Ŝalkus *et al.* 2013).

The frequency dependence of ac conductivity(σ vs f) at different temperatures (300 to 740K) have been plotted in Fig.8 and two regions clearly standout. The curves show plateau and frequency independent regions which are associated with dc conductivity at low frequencies and a dispersive region at high frequencies associated with short range motion of the ions as the temperature increases. At low temperatures some of the curves do not appear to obey Jonscher's power lawfully as the dispersion is only visible at the high frequency region. It is also observed that in the low frequency region (i.e., dc) the curves become narrower and show dispersion only at the high frequencies. A plateau is observed at low frequencies while at high frequencies the conductivity shows dispersion and the low frequency conductivity is frequency independent. The transition point from dc conductivity (low frequency) to ac conductivity region shifts towards higher frequencies due to increase in temperature and the ions thus gain kinetic energy making their vibrational frequency to increase (Ahmadu et al. 2011).

The frequency dependence of dielectric constant (ε" vs frequency) in the frequency range 300kHz to 3GHzand dielectric loss (ε') have been plotted in Fig.9(a-b). Fig.9(a) shows a sharp decrease in ε' to a constant value at high frequencies with increase in temperature. The dielectric constant increases with increase in temperature at low frequencies. However, at high frequencies ε' values reach a saturation point and become frequency independent. In the case of ε' the dielectric loss is higher at high temperatures and low frequencies but reaches saturation at high frequencies too. At low frequencies a dielectric dispersion is observed which strongly depends on frequency (Tellier et al. 2007). Low frequency dielectric dispersion is a common property of dielectric materials (Kobor et al. 2015). The high dielectric constant ε' at low frequencies is attributed to the contribution of charge carrier accumulation at the sample interface with the electrode (Sharma *et al.* 2009;Adnan & Mohamed 2012).

The decrease in dielectric constant ε' at high frequencies is due to the high periodic reversal of the ac field (Hegab *etal.* 2007).Fig.9(b) is similar to the behaviour of dielectric constant with frequency. The dielectric loss ε' increases with temperature and shows a high value at low frequencies due to high energy loss as a result of migration of ions in the material. As the ion in a material moves, some of its energy is lost as heat to the lattice (Sharma *et al.* 2009; Adnan & Mohamed 2012). The fact that ε' and ε" increase with temperature at low frequencies indicate that as temperature is increased the bound charge carriers get sufficient thermal energy to follow the change in external field, which in turn increases their contribution to the effect of space charge polarization and conducting ion motion(Sharma et al. 2009;Venkateswara et al. 2014).At 303 K, dielectric constant ε' *has value* ~ 40 and a maximum of 1790at 740 K, which is high compared to most reported results on NASICON compounds. Šalkus et al.(2009) reported a value of ε' ~ 17.5 at 340 K for $Li_{1.3}Al_{0.15}Y_{0.5}Ti_{1.7}(PO_4)_3$ and Ahmadu et al.(2013)reported a value of ε' ~ 20 at 310 Kand ~ 136 at 600 K for $Na_{0.25}Li_{0.75}Zr_2(PO_4)_3$. Further investigations are on the high value of the dielectric constant are required.

CONCLUSION

Stable $LiSn_{1.6}Ti_{0.4}(PO_4)_3$ceramic was

successfully synthesized using solid state reaction method. XRD analysis shows a rhombohedral R3c structure confirming the formation of the compound in coexistence withSnO_2 phase. Lattice parameters and unit cell volumes are slightly different from the pristine compound. Impedance study show the grain and grain boundary conductivities increase with increase in temperature. The conductivity–temperature study shows that the compound obeys Arrhenius law. The bulk and grain boundary activation energies were determined as 0.67eV and 0.78eV, respectively, while a high conductivity was observed at high temperatures. Conductivity and dielectric studies show that the increase in conductivity with temperature is due to increase in ion mobility. Dielectric permittivity is relatively low at 303 K with a value of ~40, whereas it is high ~790 at 740 K. These values are high compared to most reported values for NASICON materials. The results show that $LiSn_{1.60}Ti_{0.40}(PO_4)_3$may be a promising candidate for application as solid electrolyte at elevated temperatures due to the conductivity measured. However, there is need for further investigation of the high dielectric constant observed which could make it relevant for dielectric applications.

Acknowledgements

The authors acknowledge financial support from the Tertiary Education Trust Fund (**Tetfund**) under project no: TETFUND/FUTMINNA/2014/04. One of the authors, U. Ahmadu is grateful to Professor Tomas Vilnius University, Lithuania for help with Broadband impedance and dielectric spectroscopy characterisation.

REFERENCES

Adnan, S. B. R. S.,& Mohamed, N. S. 2012. Conductivity and Dielectric Studies of Li_2ZnSiO_4Ceramic Electrolyte Synthesized via Sol Gel Method. *International of Journal Electrochemical Science,* 7: 9844 –9858.

Ahmadu, U., Musa, A. O., Jonah, S. A.,& Isah, K.U. 2009. Research and development In Nigeria: A survey of facilities, problems and institutional issues in the Synthesis and characterization of sodium superionic conductor, NASICON, $Na_{1-x}L_xZr_2(PO_4)_3$, *Technology of Science Africana Journal, 4:*32-40.

Ahmadu, U.2010. Synthesis, Structure and Electrical Properties of Sodium Zirconium Phosphate $Na_{1x}Li_xZr_2(PO_4)_3$ (x=0.00-0.75),Ph.D.Dissertation,Ahmadu Bello University, Zaria,206pp.

Ahmadu, U., Musa, A. O., Jonah, S. A., Rabiu, N. 2010. Synthesis and Thermal Characterization ofNZP compounds $Na_{1-x}Li_xZr_2(PO_4)_3$ (x = 0.00-0.75). *J. Therm. Anal. Cal.*101: 175-179.

Ahmadu, U., Salkus, T., Musa, A. O., Jonah, S. A., &Isah, K.U. 2011. Electrical and Dielectric Characterisation of $Na_{0.5}Li_{0.5}Zr_2(PO_4)_3$,*Open Journal of Physical Chemistry,* 1:94-103.

Ahmadu, U., Tomas, S., Jonah, S. A., Musa, A. O., &Rabiu, N. 2013. Equivalent circuit models and analysis of impedance spectra of solid electrolyte $Na_{0.25}Li_{0.75}Zr_2(PO_4)_3$, *Advanced Materials Letters,* **4:** 185-195.

Ahmadu, U.2014. NASICON: Synthesis, Structure and Electrical Characterisation, in: Advanced Sensor and Detection Materials, edited by A. Tiwari & M. Mustafa Demir, WILEY-Scrivener publishing, U.S.A.pp.265-300.

Aono, E. H., Sugimoto, Y., Sadaoka, N., Imanaka, N.,& Adachi, G. 1993. Ionic Conductivity of Solid Electrolytes Based on Lithium Titanium Phosphate. *Solid State Ionics,*38: 4041.

Bonanos, N., Steel,B. C. H. and Butler,E. P.2005. Microstructural Models for Impedance Spectra ofMaterials in:*Impedance Spectroscopy Theory, Experiment, and Applications, Second Edition edited by E.* Barsoukov & J. R. Macdonald, A John Wiley &

Sons, New Jersey, USA pp1-47.
Chen, M., Kim, B.H., Xu, Q., Ahn, B.K., Kang, W.J.,& Huang, D.P. 2009. Synthesis and Electrical properties of $Ce_{0.8}Sn_{0.2}O_{1.9}$ Ceramics for IT-SODC Electrolytes by Ureacombustion Techniques. *Ceramics International*, 35:1335-1343.
Cui, W.J., Yi, J., Chen, L., Wang, C. X.,& Xia, Y.Y. 2012. Synthesis and Electrochemical characteristics of NASICON – Structure $LiSn_2(PO_4)_3$ anode material forlithium–ionbatteries. *Journal Power Sources*, 217: 77.
Hegab, N. A., Bekheet, M. A., Afifi, M. A., Wahaba, L. A.,& Shedhata, H. A. 2007. Effect of Cd Addition on the ac Conductivity and Dielectric Properties of Ge70Te30 Films. *Journal OvonicResearch*, 3: 71-82.
Ignaszak, A., Pasierb, P., Gajerski, R., & Komornicki, S. 2006. Synthesis and Properties of NASICON-type materials. *ThermochimicaActa*, 426: 7-14.
Kezionis, A., Kazakevicius, E., Salkus, T.& Orliukas, A.2011.Broadband high frequency impedance spectrometer with working temperatures up to 1200 K. *Solid State Ionics*, 188: 10-113.
Kobor, D., Bodian, O., Waly, B., Diallo, A.K.,& Tine, M. 2015. Structural and Impedance characterization of ceramics prepared from NPK fertilizer. Processing and Application of Ceramics, 9:107-115.
Krok, F., & Bruce, P. G. (1987). Characterisation of the electrode/electrolyte interfaces in cells of the type
$Li/PEOLiCF_3SO_3/V_6O_{13}$ by ac impedance methods. *Solid State Ionics*, 36: 171-174.
Kumar, P. P.,& Yashonah, S. 2006. Ionic conduction in solid state. *Journalon Chemical Science*, 118:135-154.
Lakshmi, V.,& Govindaraj, G. 2009.Impedance spectroscopic studies of planetary ball-milled lithium titanium phosphate material. Physics B, *Condensed Matter*, 404:3539–3543.
Mariappan, C.,& Govindaraj, G.2005.Conductivity and ion dynamic studies in the $Na_{1+x}Ti_{1.3-x}(PO_4)_{3-x}$ ($0 \leq x \leq 0.6$) NASICON material. *Solid State Ionics*, 176:1311-1318.
Martinez, A., Rojo, J.M., Iglesias, J.E., Sanz, J.,& Rojas, R.M.1994. Formation Process of $LiSn_2(PO_4)_3$& a
Monoclinically Distorted NASICON-Type Structure. *Chemical Material Society*,6:1790-1795.
Martinez, A., Rojo, J.M., Iglesias, J.E.,& Sanz, J. 1995. Reversible monoclinic rhombohedral transformation in $LiSn_2(PO_4)_3$ with NASICON – Type structure. *Journal of Chemical Material Society*,7:1857.
Martinez, J.A., Amarilla, J.M., Iglesias, J.E.,& Rojo, J.M.1997. Ionic conductivity of $LiHf_2(PO_4)_3$ NASICON type structure and its Possible Application as Electrolyte in Lithium Batteries. *Journal of Chemical Society*, 8:261-264.
Martinez, J. A., Jimenez, R., Martin, P. D., Ibanez, J.,& Rojo, J.M. 1997. *Effect of the phase transition of $LiSn_2(PO_4)_3$ on the Li^+ ion conduction in $LiSn_2(PO_4)_3$-Teflon composites. Journal of Physics Condensed Matter, 9:4119.*
Mustaffa, N.A., & Mohamed, N.S.2015. Properties of Stannum Based NASICON structured Solid Electrolytes for potentials application in Electrochemical Devices. *International Journal of Electrochemical Science*, 10, 5382 – 5394.
Mustaffa, N. A., Adnan, S. B. R. S., Sulaiman, M., & Mohamed, N. S. 2014. Low Temperature sintering effects on NASICON-structured $LiSn_2P_3O_{12}$ solid electrolytes prepared via citric acid-assisted sol-gel method. *International Journal of Solid State Ionics*, 21:955-965.
Narvaez-Semanate, J. L.,& Rodrigues, A. C. M. 2010. **Microstructure and ionic conductivity of$Li_{1+x}Al_xTi_{2-x}(PO_4)_3$ NASICON glass-ceramics**. *Solid State Ionics*, 181:1197-1204.
Norhaniza, R., Subban, R.H.Y., &Mohamed, N.S. 2010. Effecting of sinteringTemperature

on the structure and conductivity of $LiSn_2(PO_4)_3$ prepared by Mechanical milling method. *Advanced Material Research*,338:129-131.

Norhaniza, R., Subban, R.H.Y., & Mohamed, N.S. 2011. Ion conduction in Vanadium-substituted $LiSn_2(PO_4)_3$. *Journal of Materials Science*, 46:7815-7821.

Orliukas, A.F., Dindune, A., Kanepe, Z., Ronis, J., Bagdonas, B., & Kezionis, A. 2006.**Synthesis and peculiarities of electric properties of $Li_{1.3}Zr_{1.4}Ti_{0.3}Al_{0.3}(PO_4)_3$ solid electrolyte ceramics**. *ElectrochemicalActa*, 51:6194.

Šalkus, T.,Kazakevicus, E., Kezionis, A., Dindune, A., Kanepe, Z., Ronis, J., Emery, J., Boulant, A, Bohnke, A., & Orliukas, A. F. 2009. Peculiarities of ionic transport in $Li_{1.3}Al_{0.15}Y_{0.15}Ti_{1.7}(PO_4)_3$ ceramics. *Journal of Physics Condensed Matter*, 21:5502.

Šalkus, T., Steins, I., Barre, M., Kezionis, A.,&Orliukas, A. F. 2013. Preparation ofSuperionic Ceramics by Spark Plasma Method. *Materials Science(Medziagofyra)*,19:1392-1320.

Sharma, M. V. N. V. D., Sarma, A. V., & Rao, R. B. 2009. Electrical Characterization and Relaxation Behavior of Lithium-Indium-Phosphate Glasses via Impedance Spectroscopy. *Turkey Journal of Physics, 33:87-100.*

Tellier, J., Boullay, P.H., Jennet, D.B.,& Mercurio, D.2007. Structural versus Relaxorproperties in Aurivillius type of compound. Journal of European Ceramic Society, 27:3687-3690.

Venkateswara, A.R., Veeraiah, V.A., Prasada, V.R., Kishore, B.B., &Brahmayya, M.2014.Spectroscopic characterization and conductivity of Sn substituted $LiTi_2(PO_4)$ *Research on Chemical Intermediates*,:0922-6968.

Winand, J.M., Rulmont, A.,& Tarte, P. 1991. *Journal of Solid State Chemistry*,93:341-349.

Wu, F., Liu, Y., Chen, R., Chen, S., & Wang, G. 2009. Preparation and performance of novel Li–Ti–Si–P–O–N thin-film electrolyte for thin-film lithium batteries. *Journal of Power Sources*, 189:467-470.

Zhou, M.,& Ahmed, A. 2007.Synthesis, processing and characterisation of NASICON solid electrolyte for CO_2 sensing applications. *Sensor Actuator B:Chemical*, 122:419-426.